Cell Death & Differentiation

ARTICLE

Magnesium protects against sepsis by blocking gasdermin D N-terminal-induced pyroptosis

Dingyu Wang[1] · Jiashuo Zheng[2] · Qiongyuan Hu[2] · Cheng Zhao[2] · Qianyue Chen[1] · Peiliang Shi[1] · Qin Chen[1] · Yujie Zou[1] · Dayuan Zou[1] · Qiyao Liu[1] · Jingwen Pei[1] · Xiuwen Wu[2] · Xiang Gao[1] · Jianan Ren[2] · Zhaoyu Lin[1]

Abstract

Hypomagnesemia is a significant risk factor for critically ill patients to develop sepsis, a life-threatening disease with a mortality rate over 25%. Our clinic data analysis showed that hypomagnesemia is associated with a decreased monocyte count in septic patients. At the cellular level, we found that Mg^{2+} inhibits pyroptosis. Specifically, Mg^{2+} limits the oligomerization and membrane localization of gasdermin D N-terminal (GSDMD-NT) upon the activation of either the canonical or noncanonical pyroptotic pathway. Mechanistically, we demonstrated that Ca^{2+} influx is a prerequisite for the function of GSDMD-NT. Mg^{2+} blocks Ca^{2+} influx by inhibiting the ATP-gated Ca^{2+} channel P2X7, thereby impeding the function of GSDMD-NT and inhibiting lipopolysaccharide (LPS)-induced noncanonical pyroptosis. Furthermore, Mg^{2+} administration protects mice from LPS-induced lethal septic shock. Together, our data reveal the underlying mechanism of how Mg^{2+} inhibits pyroptosis and suggest potential clinic applications of magnesium supplementation for sepsis prevention and treatment.

Introduction

Hypomagnesemia is a common feature in critically ill patients and is associated with poor clinical outcomes [1]. Patients with hypomagnesemia appear to have a longer intensive care unit (ICU) stay, longer duration of mechanical ventilation, higher risk of developing sepsis and septic shock, and higher mortality rate [2–5]. Nevertheless, due to our poor understanding of the underlying mechanisms of hypomagnesemia and the lack of pathognomonic symptoms, it is often overlooked in clinical practice [2, 6].

Mg^{2+} has anti-inflammatory properties and acts as a Ca^{2+} antagonist [7]. Whereas magnesium supplementation reduces the inflammatory response, its depletion increases susceptibility to inflammation in experimental models [8, 9]. In particular, magnesium supplementation affords significant protection against lipopolysaccharide (LPS)-induced cardiotoxicity, lung injury, and liver injury [10–12]. Although these could be attributed to the inhibitory effect of Mg^{2+} against the release of inflammatory cytokines and oxidative stress, the detailed mechanisms involved remain to be determined.

Recent studies indicated that caspase-11-mediated non-canonical pyroptosis plays a key role in LPS-induced sepsis [13]. Pyroptosis is a cell-intrinsic death mechanism activated by cytosolic danger signals that aims to remove the infected cells and simultaneously trigger an inflammatory response [14]. However, an excessive inflammatory response can damage the host organism and even cause lethal septic shock. LPS is a strong activator of pyroptosis.

These authors contributed equally: Dingyu Wang, Jiashuo Zheng

✉ Xiang Gao
  gaoxiang@nju.edu.cn

✉ Jianan Ren
  jiananr@gmail.com

✉ Zhaoyu Lin
  linzy@nju.edu.cn

1   State Key Laboratory of Pharmaceutical Biotechnology and MOE Key Laboratory of Model Animal for Disease Study, Model Animal Research Center, Nanjing University, 210000 Nanjing, China

2   Research Institute of General Surgery, Jinling Hospital, Medical School of Nanjing University, 210000 Nanjing, China

Intraperitoneal injection with high-dose LPS in mice results in acute septic shock and death, while the deletion of genes involved in the LPS-induced pyroptotic death pathway (e.g., caspase-11, gasdermin D (*Gsdmd*)) significantly enhances survival [13, 15]. Intriguingly, ablation of Toll-like receptor 4 fails to protect mice primed with Toll-like receptor 3 ligand and then challenged with LPS, whereas ablation of caspase-11 succeeds [16, 17]. Given the extensive protective effect of magnesium in endotoxaemia, it is worthwhile to investigate whether Mg^{2+} regulates LPS-stimulated pyroptosis.

LPS-stimulated pyroptosis is mainly mediated by mouse caspase-11 and its human counterparts, caspase-4/5 [18]. Direct binding of these caspases with intracellular LPS leads to the cleavage of GSDMD and the release of N-terminal (GSDMD-NT), which is an executor of cell pyroptosis [15, 19]. GSDMD-NT then oligomerizes and translocates to the plasma membrane and forms a pore with an inner diameter of 10–14 nm that causes cell swelling and pyroptosis [20–23]. Notably, in addition to GSDMD, caspase-4/11 also functions upstream of a canonical Nod-like receptor protein 3 (NLRP3) inflammasome; upon activation, NLRP3 recruits the adaptor protein ASC and triggers caspase-1 activation, which in turn processes the maturation of proinflammatory cytokines interleukin-1β (IL-1β) and IL-18 [13, 24, 25]. Furthermore, canonical pyroptosis, which is mediated by canonical inflammasomes, caspase-1, and GSDMD, plays a critical role in polymicrobial sepsis. Blocking this process protects mice against caecum ligation and puncture (CLP)-induced sepsis [26, 27].

In this work, we found that Mg^{2+} restrains both canonical and noncanonical pyroptosis by blocking GSDMD-NT oligomerization and membrane localization. Its potential mechanism in noncanonical pyroptosis was also investigated. Furthermore, mice intraperitoneally injected with Mg^{2+} had significantly reduced susceptibility to lethal septic shock. Collectively, these findings reflect that magnesium, as a critical macroelement, is responsible for the regulation of the immune response during infection. Correction of hypomagnesemia and proper magnesium supplementation should be beneficial to reducing the sepsis morbidity of critically ill patients.

Results

Hypomagnesemia is associated with decreased monocyte levels in septic patients

Hypomagnesemia in critically ill patients has been linked to poor clinical outcomes [1]. To confirm this in Chinese patients, clinical data were collected from the surgical ICU of Jinling Hospital, Nanjing, China. From a total of 311

patients, 32 were excluded according to the exclusion criteria. Of the 279 patients studied, 136 (48.7%) were traumatic patients, and 96 (34.4%) were surgical patients. At admission, 97 (34.8%) patients had hypomagnesemia and 182 (65.2%) had normomagnesemia (Table S1). There was no significant difference in age, gender, or primary disease between the two groups of patients, but hypomagnesemic patients had a higher SOFA score and APACHE II score at admission than patients with normomagnesemia ($P = 0.075$ for both scores) (Table S1). Furthermore, patients with hypomagnesemia had a significantly longer ICU length of stay, higher risk of developing sepsis, and higher mortality rate than patients with normomagnesemia (Table S1).

To further investigate the impact of hypomagnesemia on sepsis development, 87 patients diagnosed with sepsis during their ICU stay were analyzed separately. Among these patients, 39 (44.8%) had hypomagnesemia at admission. Compared to the others, these patients did not have a significantly different white blood cell (WBC) count or WBC differential at admission (Fig. 1a). However, when sepsis struck, these patients had a significantly lower monocyte percentage ($P < 0.01$); WBC count, neutrophil percentage, and lymphocyte percentage were not significantly different from the other patients (Fig. 1a). To look for a linear relationship between the serum magnesium level at admission and the monocyte percentage on the day of sepsis diagnosis, a Pearson's correlation analysis was conducted. Importantly, a significant positive correlation was found between the two parameters ($P < 0.001$, $R(85) = 0.381$) (Fig. 1b), indicating that patients with lower serum magnesium at admission might have a lower monocyte percentage when sepsis strikes.

Mg^{2+} inhibits noncanonical pyroptosis in macrophages

The above analyses implied that magnesium might be protective to the death of monocytes during sepsis. Recently, noncanonical pyroptosis was reported to play a critical role in the development of LPS-induced sepsis [13]. To examine whether Mg^{2+} is involved in the regulation of noncanonical pyroptosis, mouse immortalized bone marrow-derived macrophages (iBMDMs) were primed with Pam3CSK4 and then electroporated with LPS. We showed that cells stimulated with intracellular LPS presented robust lactate dehydrogenase (LDH) release, which was attenuated by Mg^{2+} in a concentration-dependent manner, with as low as 5 mM being effective (Fig. 2a). Furthermore, cells incubated with 20 mM Mg^{2+} did not develop the typical pyroptotic morphology with cell swelling and membrane blebbing (Fig. 2b), and propidium iodide (PI) uptake and IL-1β release were also significantly decreased (Fig. 2c, d). By contrast, 5 mM glycine, an antilytic reagent, did not

Fig. 1 Hypomagnesemia is associated with decreased monocyte level when sepsis strikes. **a** Patients developing sepsis during their ICU stay were divided into two groups according to their serum magnesium at admission. Of the 87 septic patients, 48 were normomagnesemic (0.7–1.0 mmol/L) and 39 were hypomagnesemic (<0.7 mmol/L). Box plots of white blood cell (WBC) count, neutrophil percentages, monocyte percentages, and lymphocyte percentages in these two groups of patients are shown. In the upper panels, parameters were collected at admission; in the lower panels, parameters were collected on the day of sepsis diagnosis. The center line represents the median value, the limits represent the 25th and 75th percentile, and the whiskers represent the minimum and maximum value of the distribution. $**P < 0.01$.
b Scatter plot and regression line for the regression between serum magnesium at admission and monocyte percentage on the day of sepsis diagnosis in septic patients ($n = 87$). See also Table S1. ICU intensive care unit
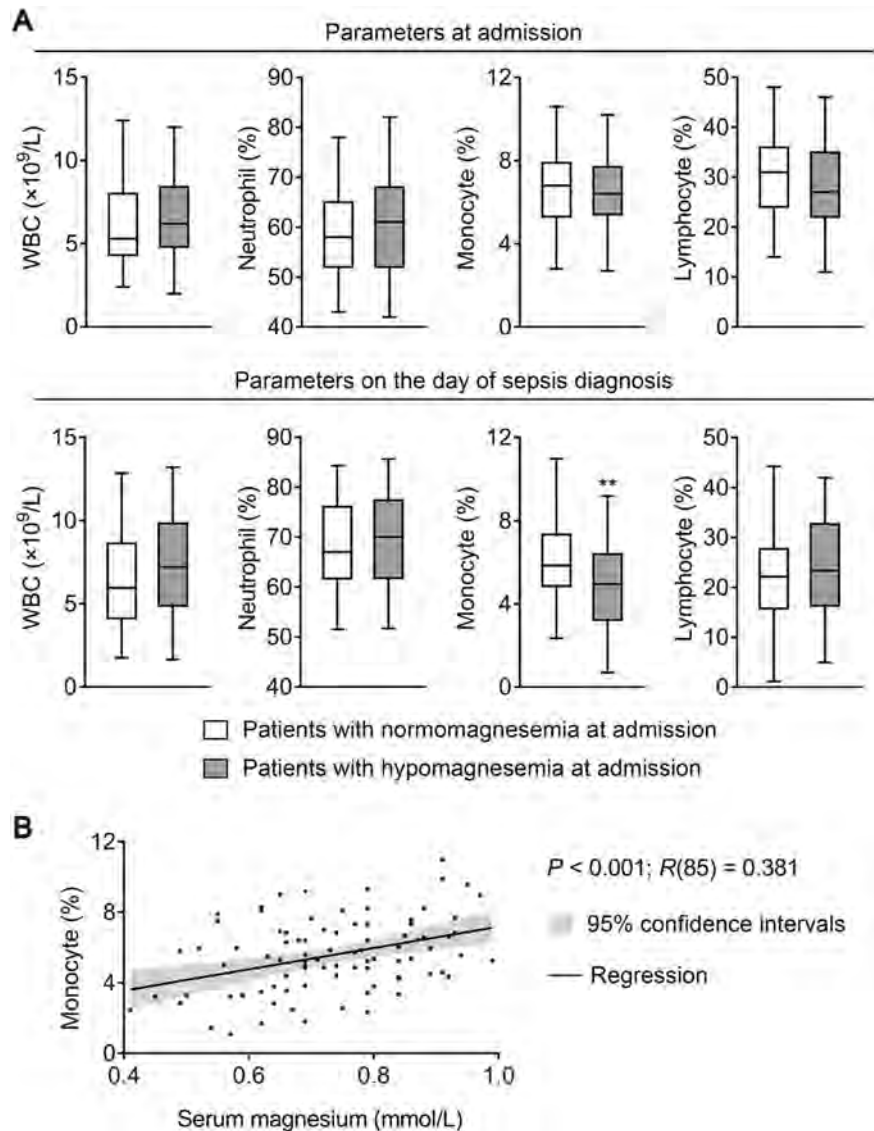

prevent the membrane blebbing, PI uptake, or IL-1β release in iBMDMs, albeit it significantly reduced the LDH release (Fig. 2a–d). These data indicated that Mg^{2+} and glycine act differently in preventing pyroptosis.

Caspase-11-mediated GSDMD cleavage is considered as a critical step in noncanonical pyroptosis [15, 19]; thus, we next examined whether GSDMD cleavage is blocked by Mg^{2+} treatment. Notably, the cleavage of GSDMD (i.e. the expression of GSDMD-NT) was not impeded (Fig. 2e). Instead, the membrane binding of GSDMD-NT was significantly blocked by Mg^{2+} (Fig. 2f). To further confirm this notion, we used different methods to separate the cytosolic and membrane fractions, and the two results were in complete agreement. In addition, Mg^{2+} did not block the activation of caspase-1, implying that the release but not maturation of IL-1β was inhibited by Mg^{2+} (Fig. 2e).

To examine whether the protective effect of Mg^{2+} on pyroptosis is cell-line specific, a similar set of experiments were conducted in human THP-1 cells which were transfected with LPS by FuGENE (Fig. S2A−E). Except that 5 mM glycine failed to reduce LDH release from THP-1 cells (Fig. S2A), the other results were in total agreement with the data in mouse iBMDMs. Together, these data indicate that Mg^{2+} inhibits noncanonical pyroptosis by impeding the membrane localization of GSDMD-NT, without affecting the activation of NLRP3 inflammasome.

Mg^{2+} inhibits canonical pyroptosis in macrophages

Given that GSDMD-NT is indispensable for both noncanonical and canonical pyroptosis [14, 15, 19, 28] while Mg^{2+} impedes the function of GSDMD-NT, we assumed that Mg^{2+} also restrained canonical pyroptosis. We first
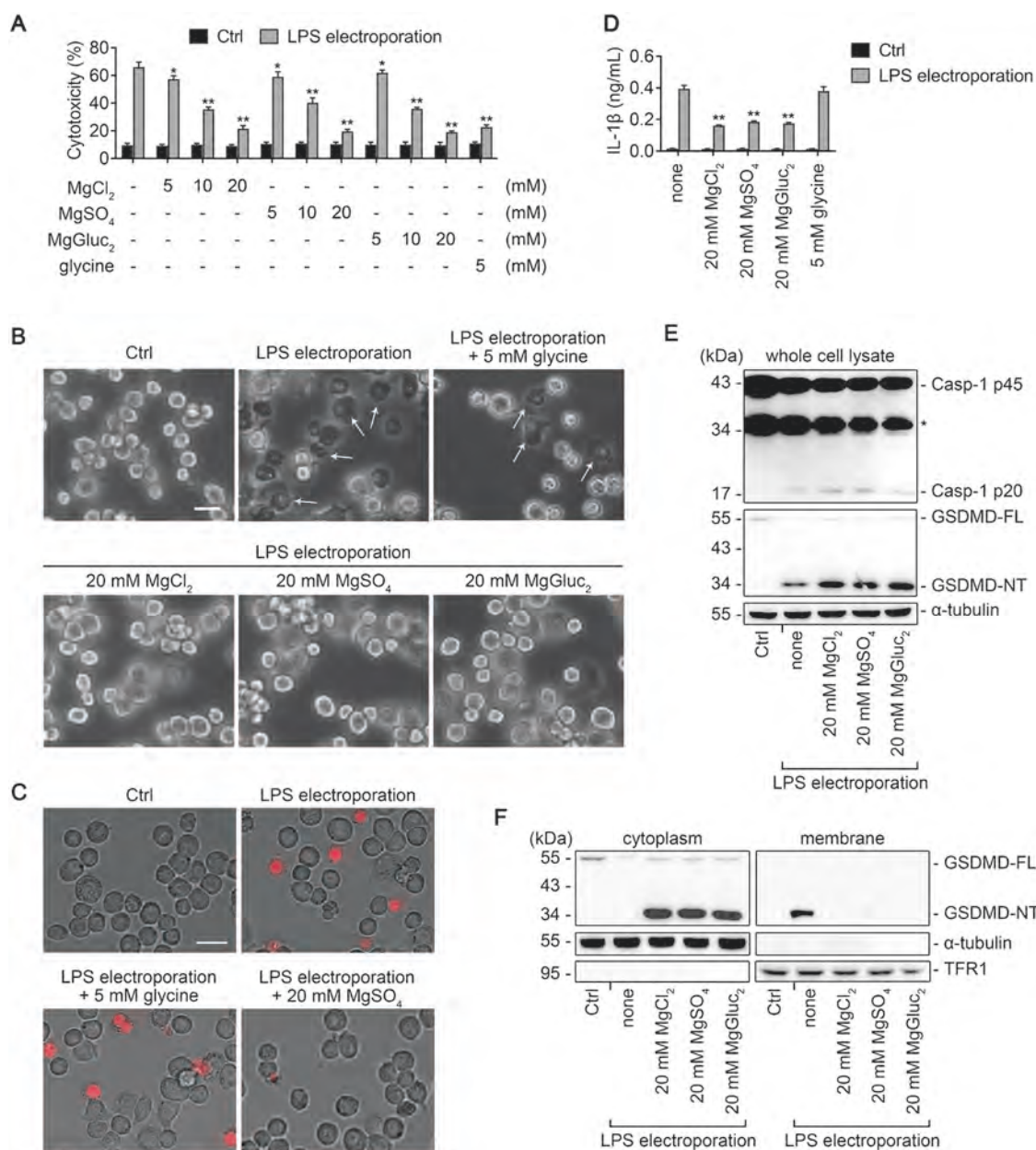
Fig. 2 Mg^{2+} inhibits noncanonical pyroptosis in iBMDMs downstream of GSDMD cleavage. **a–f** Mouse immortalized bone marrow-derived macrophages (iBMDMs) primed overnight with Pam3CSK4 in advance were electroporated with LPS for 2 h, in the absence or presence of MgCl$_2$, MgSO$_4$, MgGluc$_2$, or 5 mM glycine as indicated. Cells electroporated without LPS (Ctrl) are used as controls. **a** Percentage of LDH release (used to measure cytotoxicity). **b** Representative brightfield cell images. Representative pyroptotic cells were indicated with white arrows. Bar = 20 μm. **c** Representative images of propidium iodide (red) uptake. Bar = 20 μm. **d** IL-1β release. **e** Immunoblots for pro-caspase-1 (Casp-1 p45) and its cleavage product (Casp-1 p20), and full-length gasdermin D (GSDMD-FL) and its N-terminal (GSDMD-NT) in whole cell lysate. α-tubulin is used as a loading control. **f** Immunoblots for GSDMD-NT in the cytosolic and membrane fractions. Cytosolic and membrane-bound proteins were separated by using a Plasma membrane protein isolation kit (see Methods). α-tubulin and transferrin receptor 1 (TFR1) are used as loading controls respectively. For panels (**a**) and (**d**), data are presented as mean ± SD; *$P < 0.05$, **$P < 0.01$, compared to the cells electroporated with LPS in the absence of Mg^{2+} and glycine. Each panel is a representative experiment of at least three replicates. See also Figs. S1 and S2. LPS lipopolysaccharide, LDH lactate dehydrogenase

used LPS plus ATP to trigger canonical pyroptosis in iBMDMs, and the inhibitory effect of Mg^{2+} was confirmed by both LDH assay and morphological observation (Fig. S3A and S3B). However, since Mg^{2+} binds to ATP as evidenced by the earlier studies [29, 30], it functioned upstream of NLRP3 activation and thus blocked ASC oligomerization, caspase-1 activation, GSDMD cleavage, and IL-1β maturation and release (Fig. S3C−E). Therefore, we cannot observe the effect of Mg^{2+} on GSDMD-NT in this case.
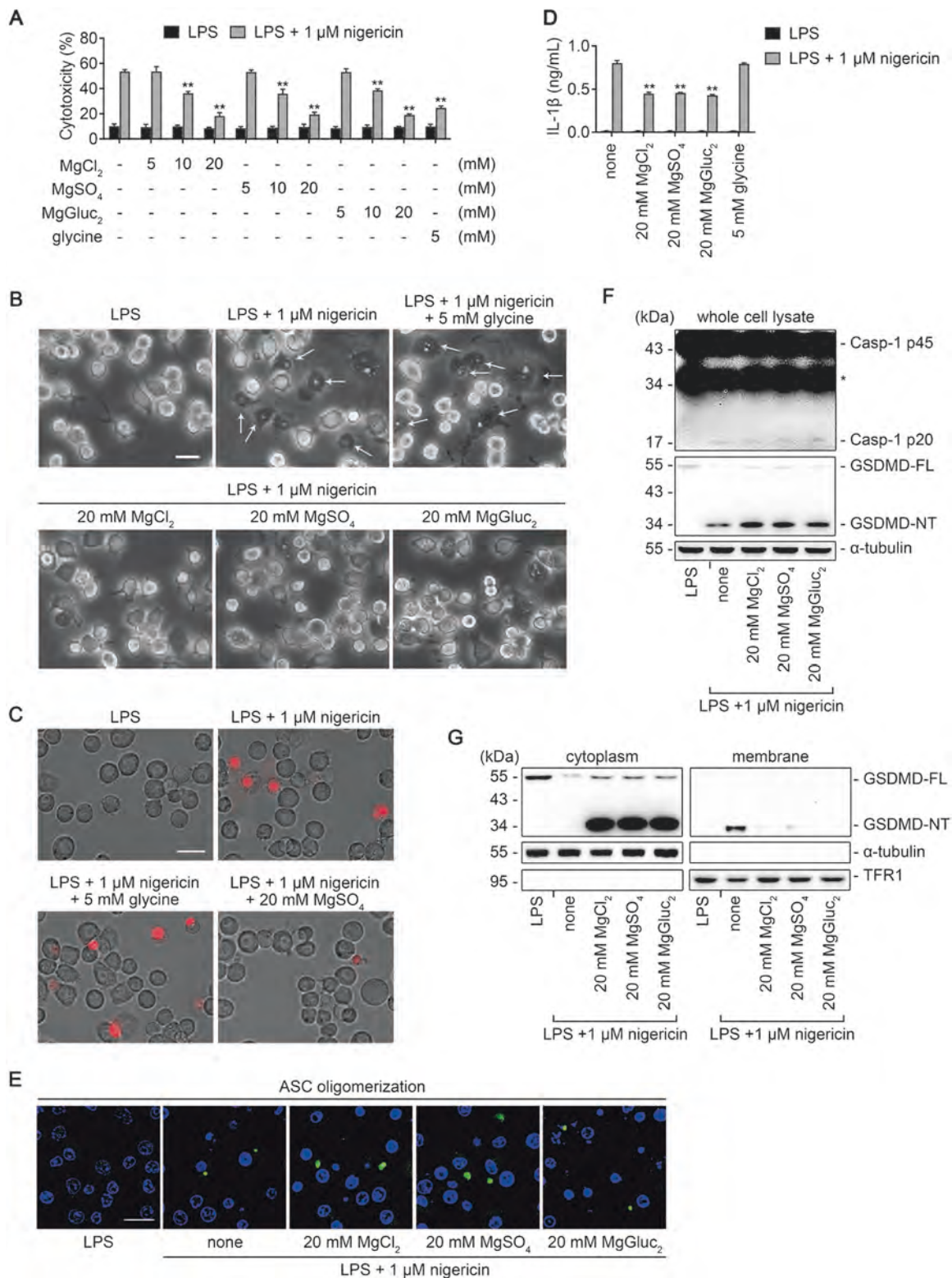
Nigericin is a K^+ ionophore that activates the NLRP3 inflammasome by depleting cytosolic K^+ [31]. We showed that Mg^{2+} also inhibited nigericin-induced pyroptosis in a concentration-dependent manner as measured by LDH release, and that 20 mM Mg^{2+} significantly prevented the membrane blebbing and PI uptake in iBMDMs in response to nigericin stimulation (Fig. 3a–c). Importantly, IL-1β release was decreased while ASC oligomerization, caspase-

1 activation, or GSDMD cleavage were not affected by Mg^{2+} (Fig. 3d–f). Further analysis indicated that Mg^{2+} blocked the membrane binding of GSDMD-NT (Fig. 3g and Fig. S4), consistent with the results in noncanonical pyroptosis. Together, these data confirm that the inhibitory effect of Mg^{2+} on the membrane binding of GSDMD-NT exists not only in noncanonical pyroptosis but also in canonical pyroptosis.

Mg^{2+} inhibits GSDMD-NT membrane binding and oligomerization in HEK293T cells

GSDMD-NT oligomerizes on the plasma membrane during pyroptosis [20, 22]; thus, we used HEK293T cells to determine whether GSDMD-NT oligomerization is blocked by Mg^{2+}. HEK293T cells transfected with human *GSDMD-NT* cDNA were largely killed, displaying pyroptotic morphology and robust LDH release, but these were significantly abrogated by Mg^{2+} (Fig. 4a and Fig. S5). Further analysis indicated that the membrane localization, but not the expression, of GSDMD-NT was inhibited (Fig. 4b), and these results were visualized in HEK293T cells expressing enhanced green fluorescent protein (eGFP)-labeled GSDMD-NT (Fig. 4c). To detect oligomer formation, HEK293T cells expressing Flag-GSDMD-NT were lysed under nonreducing conditions, and Flag immunoblot was performed. Consistent with a previous report [22], GSDMD-NT oligomers were detected at >180 kDa on a nonreducing gel, and the band disappeared in the presence of Mg^{2+}, suggesting that Mg^{2+} inhibits GSDMD-NT oligomerization (Fig. 4d). To further confirm this, GSDMD-NT was labeled with cyan fluorescent protein (CFP) or yellow fluorescent protein (YFP) to record fluorescence resonance energy transfer (FRET). We first demonstrated

that these tagged proteins were still functional in the absence but not presence of Mg^{2+} (Fig. S6A and S6B). FRET experiments were then performed to examine their interactions. Whereas the FRET signals could barely be determined in the presence of Mg^{2+}, robust signals emerged after a brief washout (Fig. 4e). The quantification of these signals indicated a significant increase in FRET efficiency after the washout, confirming that GSDMD-NT oligomerization is blocked by Mg^{2+} (Fig. 4f). Taken together, our results demonstrate that both membrane localization and oligomerization of GSDMD-NT are blocked by Mg^{2+}.

Mg^{2+} inhibits GSDMD-NT-induced pyroptosis by blocking Ca^{2+} influx

Mg^{2+} is a powerful Ca^{2+} antagonist physiologically [7], and we next investigated whether the inhibitory effect of Mg^{2+} on GSDMD-NT was associated with its role as a Ca^{2+} antagonist. Interestingly, EGTA, a selective chelator of extracellular Ca^{2+}, and BAPTA-AM, a strong chelator of intracellular Ca^{2+}, both significantly inhibited GSDMD-NT-induced pyroptosis in HEK293T cells (Fig. 5a). Similar effects were observed in cells treated with lanthanides (La^{3+} and Gd^{3+}), which are broad-spectrum inhibitors of cation channels, and in cells incubated with Ca^{2+}/Mg^{2+}-free medium or Ca^{2+}-free medium (Ca^{2+}/Mg^{2+}-free medium supplemented with 0.8 mM Mg^{2+}) (Fig. 5a). These data indicate that blocking Ca^{2+} influx could also rescue GSDMD-NT-induced pyroptosis.

To directly demonstrate that Mg^{2+} inhibits GSDMD-NT-induced pyroptosis via blocking Ca^{2+} influx, human GSDMD-NT was inducibly expressed in HEK293T cells, and GCaMP6 plasmid, a genetically encoded Ca^{2+} indicator, was used to monitor the Ca^{2+} level in live cells. We noticed that the fluorescence intensity of GCaMP6 was markedly increased in the absence, but not presence, of Mg^{2+} (Fig. 5b and Video S1). Further analysis revealed that the Ca^{2+} signal emerged much earlier than LDH release (Fig. 5c, d), consistent with the previous report [32]. Additionally, the membrane localization of GSDMD-NT was impeded when Ca^{2+} was removed (Fig. 5e), and both intracellular LPS- and nigericin-induced pyroptosis were blocked when cells were cultured in Ca^{2+}/Mg^{2+}-free or Ca^{2+}-free medium (Fig. 5f, g). Collectively, these data indicate that Ca^{2+} influx is essential for GSDMD-NT-induced pyroptosis and that Mg^{2+} inhibits Ca^{2+} influx and thereby blocks pyroptosis.

The ATP-gated Ca^{2+} channel P2X7 is essential for noncanonical pyroptosis

To determine which type of Ca^{2+} channel is involved in noncanonical pyroptosis, iBMDMs electroporated with LPS
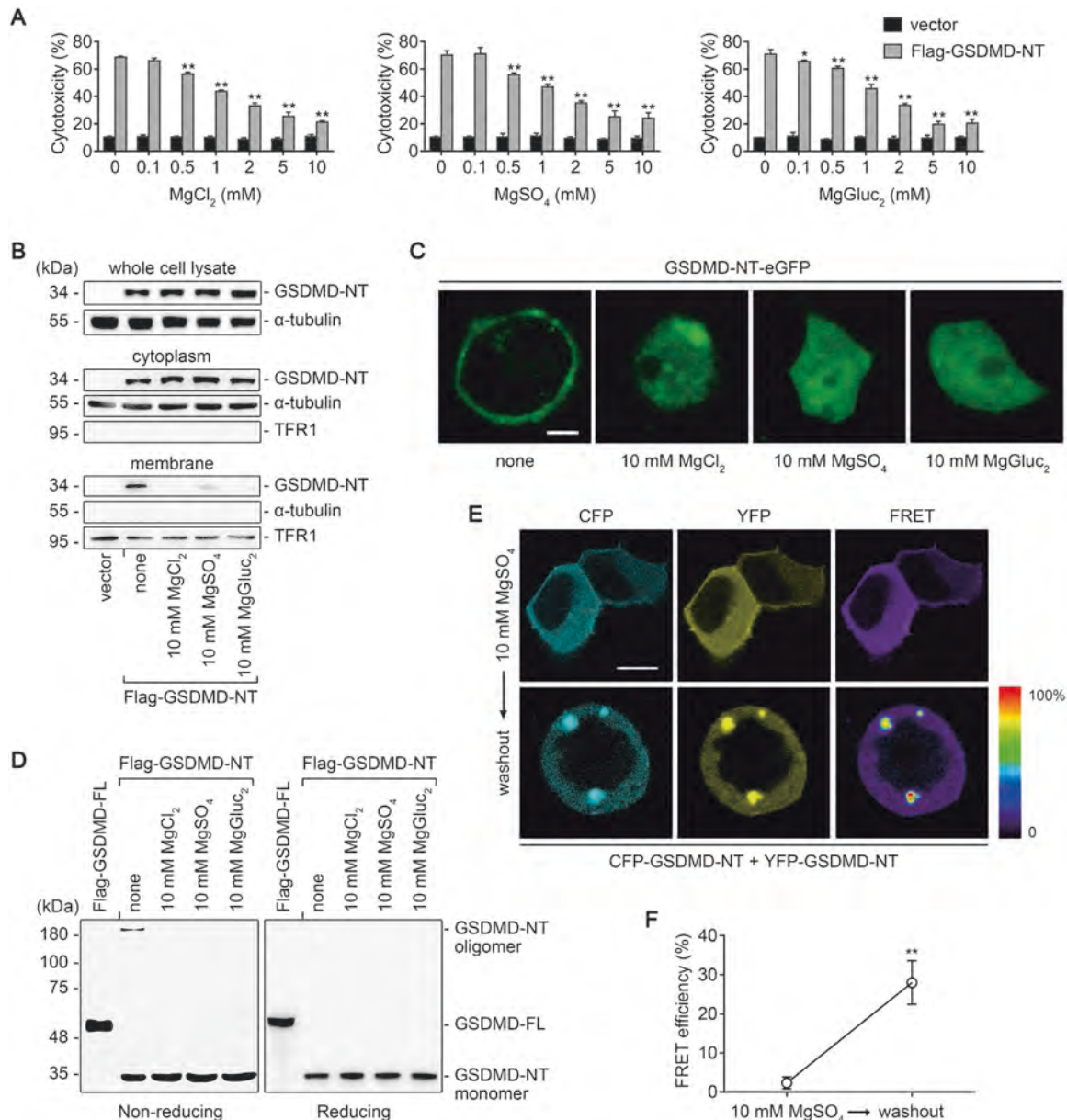
Fig. 4 Mg^{2+} inhibits GSDMD-NT membrane localization and oligomerization in HEK293T cells. **a–f** HEK293T cells transfected with indicated cDNA were cultured for 16 h, in the absence or presence of $MgCl_2$, $MgSO_4$, or $MgGluc_2$ as indicated. **a** Percentage of LDH release. **b** Immunoblots for Flag in the whole cell lysate, cytosolic fraction, and membrane fraction. Cytosolic and membrane-bound proteins were separated by using a Plasma membrane protein isolation kit. α-tubulin and TFR1 are used as loading controls respectively. **c** Representative confocal immunofluorescence images of cells. Bar = 5 μm. **d** Oligomer formation assessed by Flag immunoblot of non-reducing gel (left) and reducing gel (right). **e, f** Cells transfected with CFP-GSDMD-NT and YFP-GSDMD-NT were cultured for 16 h in the presence of 10 mM $MgSO_4$. The fluorescence resonance energy transfer (FRET) signal was then detected before and after a washout of $MgSO_4$. Shown are representative images (**e**) and quantification of FRET efficiency (**f**). Bar = 10 μm. For panels (**a**) and (**f**), data are presented as mean ± SD; *$P < 0.05$, **$P < 0.01$, compared to the cells transfected with Flag-GSDMD-NT in the absence of Mg^{2+} (**a**) or the cells before the washout (**f**). Each panel is a representative experiment of at least three replicates. See also Figs. S5 and S6. LDH lactate dehydrogenase

were treated with various Ca^{2+} channel blockers. Four types of voltage-dependent Ca^{2+} channel blockers, including nifedipine, mibefradil, amlodipine, and manidipine, all failed to rescue the cells (Fig. 6a). By contrast, two types of broad-spectrum Ca^{2+} channel blockers, La^{3+} and Gd^{3+}, succeeded (Fig. 6a).

P2X7 is a Ca^{2+} channel sensitive to La^{3+} and Gd^{3+} and has been reported to play a key role in noncanonical pyroptosis [33–35]. Ablation of P2X7 protects BMDMs against intracellular LPS stimulation [33]. Therefore, we assumed that P2X7-mediated Ca^{2+} influx is critical for the normal function of GSDMD-NT. As P2X7 is expressed in
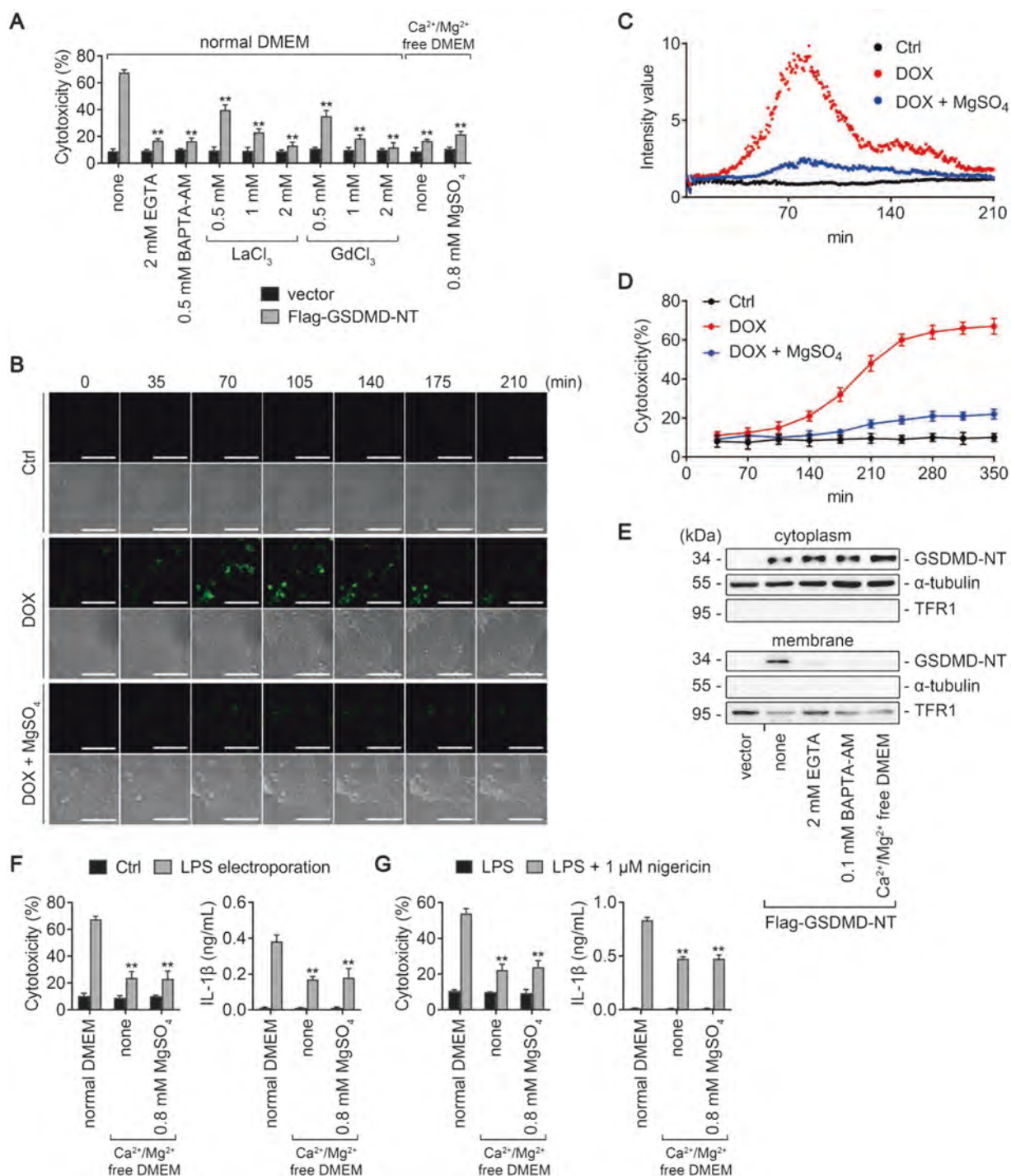
iBMDMs, we used CRISPR/Cas9 technology to knockout (KO) *P2X7* gene. Consistent with the previous study [33], *P2X7* KO iBMDMs were resistant to LPS electroporation while WT iBMDMs and *P2X7* KO iBMDMs reconstituted with plasmid producing P2X7 remained susceptible (Fig. 6b, c). Furthermore, IL-1β release was partly blocked by *P2X7* KO (Fig. 6c). These data were further confirmed by *P2X7* shRNA knockdown in iBMDMs (Fig. S7A and S7B).

P2X7 is activated by ATP released from pannexin-1 channel in noncanonical pyroptosis [33], and Mg^{2+} is an ATP chelator which can block the activation of P2X7 [29, 30]. As other divalent metal cations, such as Cu^{2+}, Zn^{2+}, Ni^{2+}, have been reported to have much higher potency than Mg^{2+} to reduce the affinity of ATP binding to P2X7 [30], we treated iBMDMs undergoing noncanonical pyroptosis with 1 mM Mg^{2+}, Cu^{2+}, Zn^{2+}, and Ni^{2+}. Whereas 1 mM Mg^{2+} basically had no effect on pyroptosis,

Fig. 5 Mg^{2+} inhibits GSDMD-NT-induced pyroptosis by blocking Ca^{2+} influx. **a**, **e** HEK293T cells transfected with Flag-GSDMD-NT (or empty vector) were treated as indicated. Percentage of LDH release was measured (**a**), and immunoblots for GSDMD-NT in the cytosolic and membrane fractions were performed (**e**). Cytosolic and membrane-bound proteins were separated by using a Plasma membrane protein isolation kit. α-tubulin and TFR1 are used as loading controls respectively. **b**−**d** HEK293T cells transduced with a doxycycline-(DOX-) inducible human GSDMD-NT cDNA were transfected with GCaMP6 plasmid, a genetically encoded Ca^{2+} indicator. Cells were treated (or untreated) with DOX 16 h later, in the absence or presence of 10 mM $MgSO_4$. **b** Representative time-lapse cell images (brightfield and fluorescence) taken from 0 to 210 min after DOX addition. Bar = 100 μm. **c** Scatter plot of the fluorescence intensity of GCaMP6. **d** LDH release measured from 35 to 350 min after DOX addition. **f** iBMDMs primed with Pam3CSK4 overnight were electroporated with (or without) LPS and incubated in the indicated media for 2 h. LDH (left) and IL-1β (right) release were measured. Cells electroporated without LPS (Ctrl) were used as controls. **g** iBMDMs primed with LPS for 4 h were treated (or untreated) with 1 μM nigericin in the indicated media for 1 h. LDH (left) and IL-1β (right) release were measured. For panels (**a**, **f**, and **g**), data are presented as mean ± SD; **$P < 0.01$, compared to the cells transfected with Flag-GSDMD-NT (**a**), electroporated with LPS (**f**), or treated with nigericin (**g**) in normal DMEM. Each panel is a representative experiment of at least three replicates. See also Video S1. LPS lipopolysaccharide, iBMDM immortalized bone marrow-derived macrophage, DMEM Dulbecco's modified Eagle's medium

1 mM Cu^{2+}, Zn^{2+}, and Ni^{2+} significantly reduced the LDH release and impeded the membrane binding of GSDMD-NT (Fig. 6d, e), similar to the effect of 20 mM Mg^{2+}.

Furthermore, consistent with the previous report [33], both pannexin-1 inhibitors (carbonoxolone, probenecid, and trovafloxacin) and P2X7 inhibitors (A438079, A740003, and A804598) rescued iBMDMs electroporated with LPS, while only pannexin-1 inhibitors completely blocked the cleavage of caspase-1 and the release of IL-1β (Fig. 6f, g). Notably, blockade of either pannexin-1 or P2X7 had no impact on the cleavage of GSDMD but impeded the membrane localization of GSDMD-NT (Fig. 6g). These data suggest that P2X7-mediated Ca^{2+} influx is crucial for the membrane localization of GSDMD-NT to induce noncanonical pyroptosis.

Mg^{2+} protects against LPS-induced septic shock

To extend our in vitro findings, we next examined whether Mg^{2+} solutions could protect mice from LPS-induced septic shock. Mice were primed with 0.4 mg/kg LPS and then challenged with 10 mg/kg LPS 6 h later. In agreement with a previous study [33], wild-type mice that were treated with 0.9% NaCl (LPS group) succumbed within 24 h; whereas over 50% of mice that were treated with 1 mmol/kg Mg^{2+} survived beyond 72 h (Fig. 7a). Under the protection of Mg^{2+}, the amount of serum IL-1β and IL-6 at 4 and 8 h after LPS challenge was significantly reduced, confirming the anti-inflammatory effects of Mg^{2+} (Fig. 7b). Other cytokines (e.g., TNF-α, IL-2, IL-4, IL-5, IL-10, IL-12p70, and

IFN-γ), however, were not significantly different between the two groups (Fig. 7b and Fig. S8A). By routine blood test, we found that the WBC levels and WBC differential count in mice treated with Mg^{2+} were significantly higher than in the LPS group after LPS challenge (Fig. 7c). In particular, the monocyte count in mice treated with Mg^{2+} was twice that in the LPS group (Fig. 7c). Consistent with this finding, flow cytometry analysis showed that mice treated with Mg^{2+} had apparently higher monocyte and macrophage percentages than those in the LPS group (Fig. 7d), whereas T cell, B cell, and nature killer cell percentages were comparable between the two groups (Fig. S8B). LPS-induced endothelial pyroptosis is the leading cause of death in endotoxaemic mouse models [36]. By H&E staining, we observed that Mg^{2+} markedly alleviated the inflammation and lung injury caused by LPS challenge in lung (Fig. 7e), which is in accord with a previous report [10]. Collectively, these results suggest that Mg^{2+} might be protective in LPS-induced septic shock; the underlying mechanisms might be associated with its inhibitory effect on pyroptosis and on the release of proinflammatory cytokines.

Discussion

Magnesium homeostasis is essential for the physiological function of multiple organs, and magnesium supplementation has been considered as a treatment for several major diseases, such as preeclampsia, migraine, depression, and asthma [7]. However, modest hypomagnesemia is often neglected in clinical practice due to the lack of characteristic clinical features [7]. Several studies, along with our current work, indicate that critically ill patients with hypomagnesemia have a higher risk of developing sepsis than patients with normomagnesemia [2–5]. This is probably because hypomagnesemia makes cells more susceptible to pyroptosis. When infection occurs, cells are excessively activated, resulting in extensive pyroptosis and robust inflammatory response. Our data indicate that Mg^{2+} is essential for protecting cells from pyroptosis, and the magnesium level is an important index for critically ill patients.

Mg^{2+} acts as a physiological Ca^{2+} antagonist, and changes in intracellular and extracellular Mg^{2+} concentration often cause disturbed Ca^{2+} signaling [7]. In this study, we proposed that Mg^{2+} impeded pyroptosis by blocking Ca^{2+} influx. In noncanonical pyroptosis, caspase-11-dependent cleavage of pannexin-1 leads to ATP release, which in turn activates P2X7, a Ca^{2+} channel, to mediate pyroptosis [33]. We showed that extracellular Mg^{2+} bound to ATP and thereby impeded the activation of P2X7 as well as P2X7-mediated Ca^{2+} influx, and that the ATP-gated Ca^{2+} channel P2X7 is indispensable for noncanonical
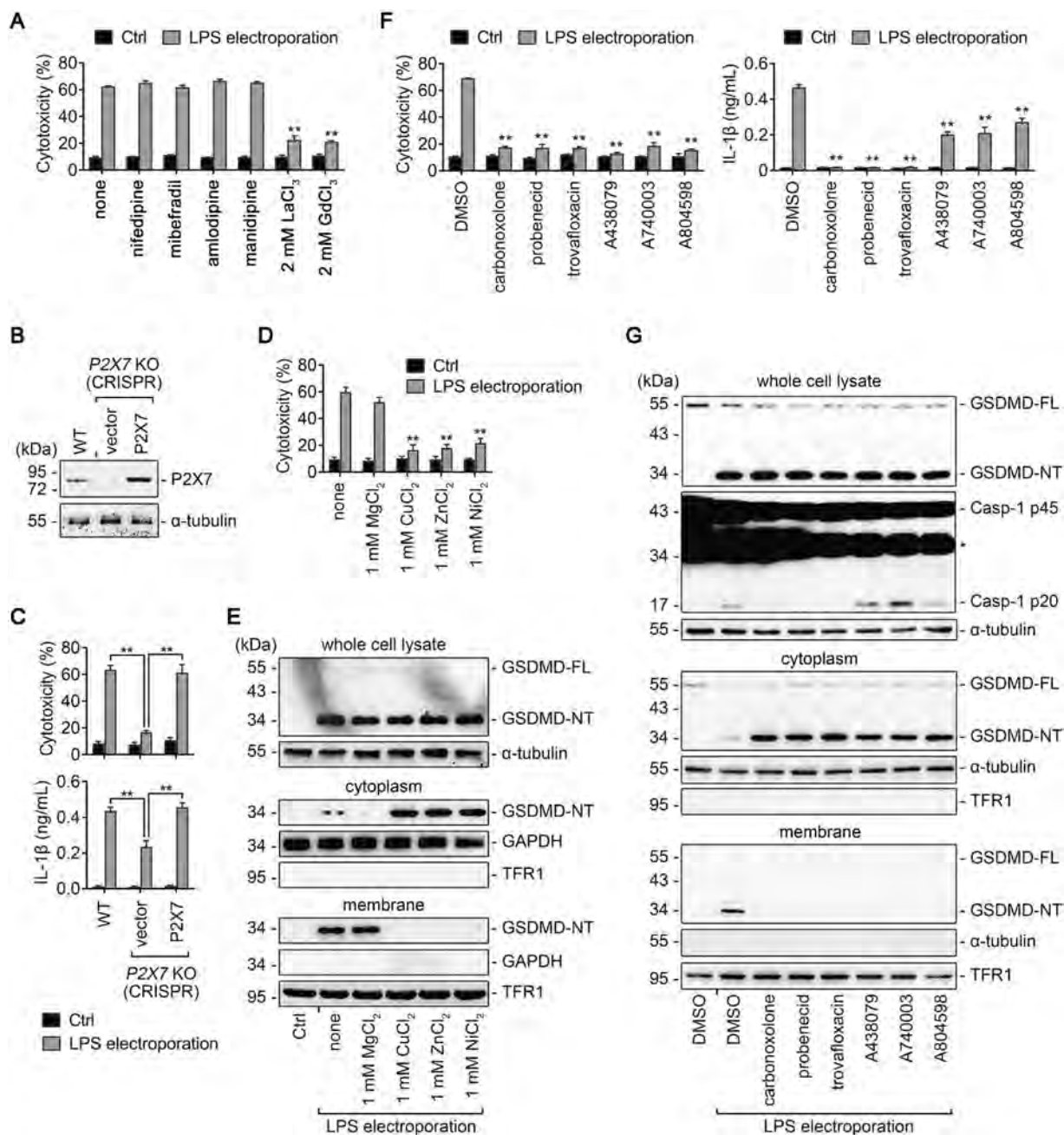
Fig. 6 The ATP-gated Ca^{2+} channel P2X7 is essential for non-canonical pyroptosis. **a**, **c**−**g** iBMDMs primed overnight with Pam3CSK4 in advance were electroporated with LPS for 2 h. Cells electroporated without LPS (Ctrl) are used as controls. Ca^{2+} channel inhibitors (i.e. nifedipine, mibefradil, amlodipine, manidipine, $LaCl_3$, $GdCl_3$), pannexin-1 inhibitors (i.e., carbonoxolone, probenecid, and trovafloxacin), and P2X7 inhibitors (i.e., A438079, A740003, and A804598) were added 30 min before the electroporation, while $MgCl_2$, $CuCl_2$, $ZnCl_2$, and $NiCl_2$ were added right after the electroporation. The concentration of the inhibitors were all 0.1 mM. **a** Percentage of LDH release from cells treated as indicated. **b** Immunoblot for P2X7 in whole-cell lysate of WT iBMDMs and *P2X7* knockout (KO) iBMDMs transfected with empty vector or *P2X7* cDNA. α-tubulin is used as a loading control. **c** WT iBMDMs and *P2X7* KO iBMDMs transfected with empty vector or *P2X7* cDNA were primed and electroporated as described above. Shown are LDH (upper) and IL-1β (lower) release. **P < 0.01. **d** Percentage of LDH release from cells treated as indicated. **e**, **g** Immunoblots for GSDMD-FL, GSDMD-NT, Casp-1 p45, Casp-1 p20 in the whole-cell lysate, cytosolic fraction, and membrane fraction of cells treated as indicated. Cytosolic and membrane-bound proteins were separated through the use of OptiPrep™ (**f**) or by using a Plasma membrane protein isolation kit (**g**). α-tubulin, glyceraldehyde 3-phosphate dehydrogenase (GAPDH), and TFR1 are used as loading controls respectively. **f** LDH (left) and IL-1β (right) released from cells treated as indicated. Data are presented as mean ± SD. For panels (**a**, **d**, and **f**), **P < 0.01, compared to the cells electroporated with LPS and then left untreated or treated with DMSO. Each panel is a representative experiment of at least three replicates. See also Fig. S7. iBMDM immortalized bone marrow-derived macrophage, LPS lipopolysaccharide, LDH lactate dehydrogenase
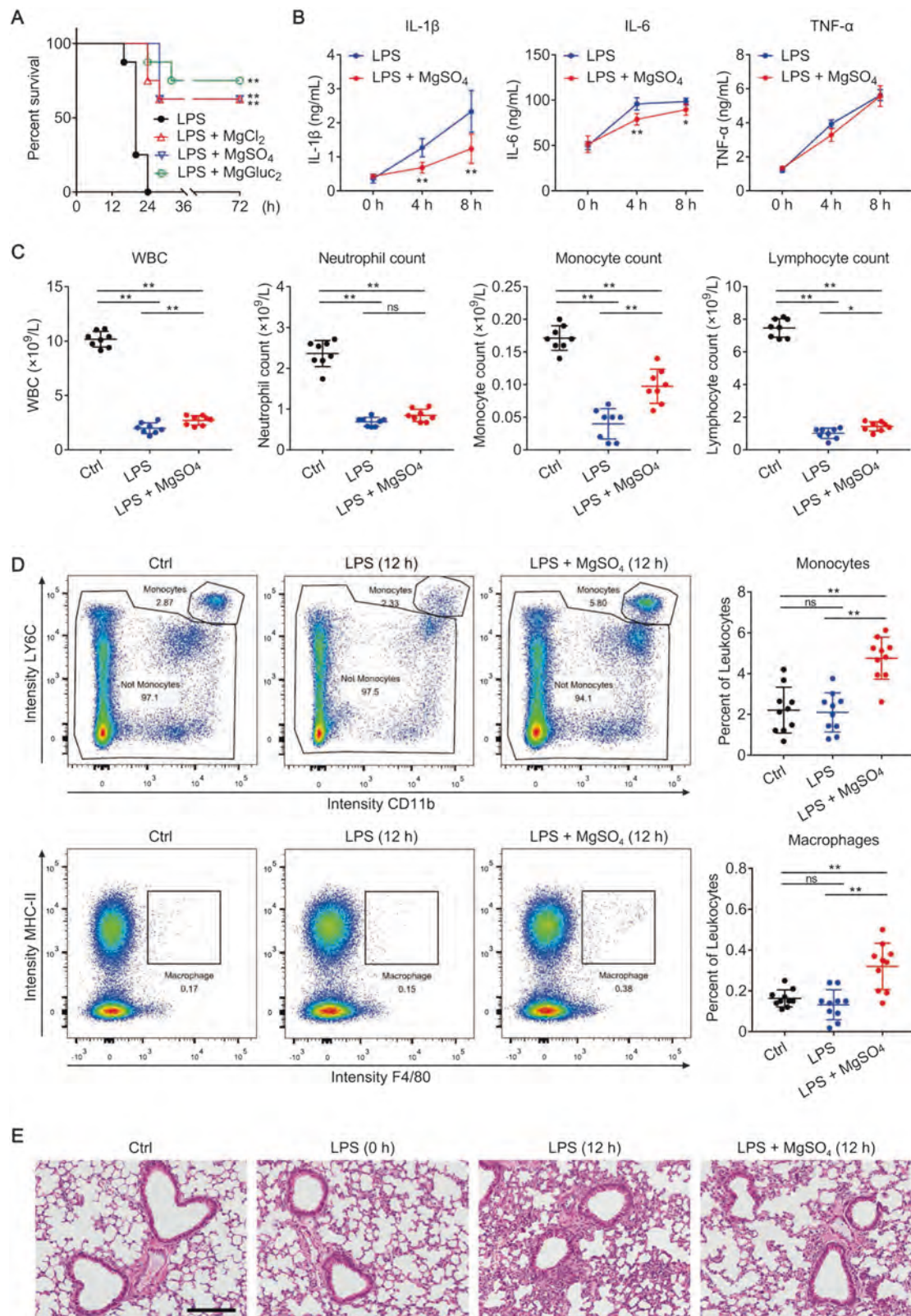
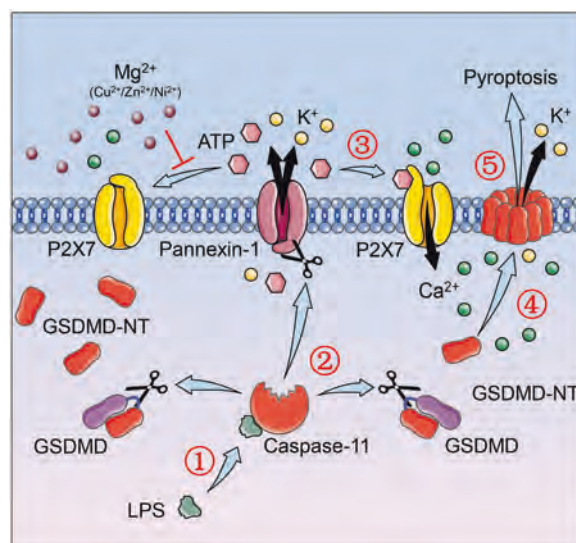pyroptosis (Fig. 8). For regulating canonical pyroptosis elicited by nigericin, however, the specific Ca^{2+} channel remains to be determined. We know this specific channel can be inhibited by Mg^{2+}, La^{3+}, and Gd^{3+}, and the channel has nothing to do with pannexin-1 or P2X7 [37, 38]. Furthermore, as P2X7 is not expressed in HEK293T cells [39],

◀ **Fig. 7** Mg^{2+} is protective in LPS-induced endotoxic shock. **a–e** *C57BL/6* male mice were left untreated (Ctrl group) or primed with 0.4 mg/kg *E. coli* O111:B4 LPS intraperitoneally and then challenged 6 h later with 10 mg/kg *E. coli* O111:B4 LPS intraperitoneally. Upon the secondary challenge, LPS was mixed with 1 mmol/kg $MgSO_4$, $MgCl_2$ or $MgGluc_2$ as indicated, or an equal volume of 0.9% NaCl (LPS group). $N = 8$ per group. **a** Survival of mice after LPS challenge. $**P < 0.01$, compared to the LPS group. **b** IL-1β, IL-6, and TNF-α levels in mouse plasma measured at the indicated time points after LPS challenge. Mice treated with $MgSO_4$ were compared to the LPS group at each time point. **c** Cell counts of white blood cell (WBC), neutrophil, monocyte, and lymphocyte in mouse whole blood measured in a normal state (Ctrl) or at 12 h after LPS challenge. **d** Representative flow cytometry plots (left) and quantification (right) of monocytes ($CD11b^+LY6C^+LY6G^-$) and macrophages ($CD11b^+MHC-II^+F4/80^+$) in mouse whole blood measured in a normal state (Ctrl) or at 12 h after LPS challenge. **e** Representative H&E-stained lung sections obtained from mice in a normal state (Ctrl) or at 0 or 12 h after LPS challenge. Bar = 100 μm. Data are presented as mean ± SD. $*P < 0.05$, $**P < 0.01$, ns = not significant. Each panel is a representative experiment of at least two replicates. See also Fig. S8

Fig. 8 A model regarding how Mg^{2+} impedes noncanonical pyroptosis. Upon intracellular LPS stimulation, activated caspase-11 cleaves and activates the K^+ channel pannexin-1 on the one hand, and cleaves GSDMD to form GSDMD-NT on the other. Subsequently, activated pannexin-1 releases ATP to elicit Ca^{2+} channel P2X7, which licenses the Ca^{2+} influx. With the help of Ca^{2+} influx, either directly or indirectly, GSDMD-NT then binds to the plasma membrane and oligomerizes to form pores which result in membrane rupture and pyroptosis. Meanwhile, the K^+ efflux mediated by pannexin-1 and GSDMD-NT pore, and probably the mitochondrial reactive oxygen species driven by GSDMD-NT, all contribute to the activation of NLRP3 inflammasome (not shown in the figure). Nevertheless, divalent metal cations such as Mg^{2+}, Cu^{2+}, Zn^{2+}, Ni^{2+}, may disrupt the pyroptotic process by binding to ATP. In this case, the ATP released by pannexin-1 cannot activate P2X7, and thus Ca^{2+} influx is blocked. Without Ca^{2+} influx, GSDMD-NT cannot bind to the membrane and form pores, and pyroptosis is therefore inhibited. LPS lipopolysaccharide

the Ca^{2+} influx triggered by GSDMD-NT in HEK293T cells must be mediated by other channels, probably TMEM16F [40]. However, it is still an open question as to whether TMEM16F is essential for pyroptosis in macrophages. These results indicate that although Ca^{2+} influx is essential for the function of GSDMD-NT, the specific channel may differ among various cell types and various pathways.

Notably, previous studies have showed that GSDMD pores can be assembled in synthetic liposomes in the absence of Ca^{2+} [22]. We reasoned that this discrepancy may be attributed to the different systems used. Specifically, cell is much more complicated than synthetic liposome. Indeed, it is still unclear whether Ca^{2+} assists the assembly of GSDMD-NT pore directly or indirectly, and we cannot rule out the possibility that Ca^{2+} may regulate other proteins in cells which license the assembly of GSDMD-NT. Hence, the underlying mechanism concerning how Ca^{2+} regulates GSDMD-NT pore assembly must be further investigated in the future.

Many previous studies have indicated that the ability of noncanonical inflammasome activation to secondarily activate NLRP3/caspase-1 is mediated by K^+ efflux, and that GSDMD is indispensable in this process. Nevertheless, no study, as far as we are concerned, has demonstrated that K^+ efflux is necessarily via the GSDMD-NT pore. Notably, a previous study showed that activated caspase-11 triggers the opening of the pannexin-1 channel through cleavage, which induces the K^+ efflux required for NLRP3 inflammasome activation [33]. Our data also demonstrated that pannexin-1 inhibitors completely impeded caspase-1 activation and IL-1β release. In addition, another study proposed that GSDMD-NT-induced mitochondrial reactive oxygen species (ROS) also contributed to the activation of NLRP3 inflammasome in caspase-4-mediated noncanonical

pyroptosis [41]. Pretreating cells with antioxidant *N*-acetylcysteine impeded caspase-1 cleavage and IL-1β production without affecting caspase-4 cleavage [41]. Taken together, it appears that the K^+ efflux mediated by pannexin-1 and GSDMD-NT pore, as well as the mitochondrial ROS elicited by GSDMD-NT, all contribute to NLRP3 inflammasome activation in noncanonical pyroptosis. Impeding any of these (e.g. ablation of GSDMD, inhibition of pannexin-1, blockade of the K^+ efflux, elimination of mitochondrial ROS) may affect the normal activation of NLRP3 inflammasome. In this study, we showed that Mg^{2+} impeded the membrane binding of GSDMD-NT without affecting caspase-1 activation. This may be attributed to the K^+ efflux mediated by pannexin-1 and the mitochondrial ROS mediated by GSDMD-NT. In addition, we cannot rule out the possibility that a small amount of GSDMD-NT pores generated and contributed to K^+ efflux even in the presence of 20 mM Mg^{2+}.

In summary, our current work reveals that Mg^{2+}, as a Ca^{2+} antagonist, regulates the oligomerization and membrane

localization of GSDMD-NT and thereby protects the cell from pyroptosis. The role of Ca^{2+} influx as a prerequisite for GSDMD-NT to function was proposed, and the relationship between caspase-11-pannexin-1-P2X7 signaling and caspase-11-GSDMD signaling was determined. Furthermore, our in vivo studies have demonstrated the protective effects of Mg^{2+} in an endotoxaemic mouse model. Further investigation is needed to determine whether Mg^{2+} supplementation improves the outcomes of critically ill patients.

Methods

Clinical data

Clinical data was abstracted from the medical records in surgical ICU of Jinling Hospital, Nanjing, China. All adult patients (>18 years old) admitted consecutively to the surgical ICU from January 2015 to August 2015 with available admission serum magnesium levels were primarily enrolled. Exclusion criteria were patients who presented with hypermagnesemia (serum magnesium > 1.0 mmol/L) or diagnosed with sepsis at admission, and who received magnesium supplementation during their ICU stay. The Acute Physiology And Chronic Health Evaluation (APACHE) II score and the Sequential Organ Failure Assessment (SOFA) score were determined at admission. Sepsis was diagnosed according to the diagnostic criteria of the American College of Chest Physicians/Society of Critical Care Medicine [42].

Cell culture

Human embryonic kidney (HEK) 293T cells and 293FT cells were obtained from ATCC and were cultured in Dulbecco's modified Eagle's medium (DMEM). C57BL/6 mice-derived immortalized BMDM (iBMDM) cells were kindly provided by F. Shao (National Institute of Biological Sciences, China) and THP-1 (human monocyte) cells were obtained from Shanghai Institute of Cell Biology (Shanghai, China). These two cell lines were grown in RPMI 1640 medium. In some cases, DMEM without Ca^{2+}/Mg^{2+} (Cat#SH30262.01, Hyclone) was used, and DMEM was used as control. All mediums mentioned above were supplemented with 10% fetal bovine serum (Cat#P30-3302, PANBiotech, Germany) and 1% penicillin/streptomycin. Cells of passages fewer than 15 were used for experiments. All cells were cultured at 37 °C and 5% CO_2.

Plasmids and transfection

Complementary DNA (cDNA) for human gasdermin D (GSDMD) was amplified from reverse-transcribed cDNA from THP-1 cells, and cDNA for its N-terminal (GSDMD-NT) (1–275) was derived by PCR. For transient expression in 293T cells, these two cDNAs were inserted into the NotI and XbaI sites of a pCS2 vector with an N-terminal 3× Flag epitope tag respectively; GSDMD-NT cDNA was additionally inserted into the XhoI and EcoRI sites of a pEGFP-N1 vector with a C-terminal eGFP epitope tag. For FRET experiment, CFP or YFP were inserted into the N-terminal of GSDMD-NT cDNA by homologous recombination. For Tet-On expression in 293T cells, GSDMD-NT cDNA was inserted into a pTRIPZ vector. For the plasmid harboring the GSDMD-NT gene was then cotransfected with the packing plasmids pSPAX2 and pMD2G into 293FT cells. The lentivirus particles were harvested, filtered, and concentrated by ultracentrifugation 48 h later and were used to infect 293T cells for another 48 h. 293T cells that are resistant to puromycin were selected. cDNA for mouse P2X7 was amplified from reverse-transcribed cDNA from BMDM cells, and was inserted into the EcoRI and XbaI sites of the PCS2 vector. All plasmids were verified by DNA sequencing. Lipofectamine 2000 Transfection Reagent (Invitrogen) was used for transfection.

CRISPR knockout and shRNA knockdown

To knockout P2X7 in iBMDMs, the sgRNA sequences of P2X7 (AATGGAGAGGGGCCGTTAAT and CAAAA-TAGCACCGCGCGTCC) were inserted into pSpCas9 (BB)-2A-Puro (PX459) V2.0 (#62988, Addgene). These two plasmids were electroporated using the Neon Transfection System (Invitrogen). To transiently knockdown P2X7 in iBMDMs, pLKO-1 plasmids targeting mouse P2X7 were electroporated using the Neon Transfection System (Invitrogen). The targeting sequences of P2X7 shRNA1 and P2X7 shRNA2 are CCCGGCTAC AACTTCAGATAT and GCCACAACTATACCACGAG AA, respectively.

Activation of canonical and noncanonical pyroptosis

To stimulate caspase-1-mediated canonical pyroptosis, iBMDMs were primed with 1 μg/mL LPS for 4 h followed by 5 mM ATP or 1 μM nigericin treatment for 1 h. To stimulate caspase-4/11-mediated noncanonical pyroptosis, THP-1 cells or iBMDMs were primed with 1 μg/mL Pam3CSK4 overnight and then either transfected with 2 μg/mL LPS by using 0.25% v/v FuGENE HD (Promega) or electroporated with 50 ng/mL LPS by using the Neon Transfection System (Invitrogen) following the manufacturer's instructions.

Measurement of LDH release

LDH activity in the supernatant was used to evaluate cell death. Cellular debris was removed by centrifuging the supernatant at

$300 \times g$ for 5 min. LDH measurement was performed using a CytoTox 96 Non-Radioactive Cytotoxicity Assay kit (Promega) according to the manufacturer's protocol. All values represent the percentage of LDH release by a maximum lysis control (1% Triton X-100-lysed cells).

Immunoblotting

Total cell protein was extracted on ice using RIPA lysis buffer (50 mmol/L Tris-HCl (PH 7.4), 150 mmol/L NaCl, 1% NP-40, 0.1 mmol/L ethylenediaminetetraacetic acid (EDTA), 1 mmol/L DTT with 0.4 mmol/L phenylmethanesulfonyl fluoride, 0.1 mmol/L Na_3VO_4, 0.1 mmol/L NaF and cocktail protein inhibitor). To separate cytosolic and membrane protein, two different methods were used as indicated in the relative figure legends. The first method is through the use of a plasma membrane protein isolation kit (SM-005, Invent Biotechnologies, Inc.), according to the manufacturer's instructions. The second method is through the use of OptiPrep™ Density Gradient Medium (D1556, Sigma-Aldrich) according to the protocol (Application Sheet S35; eight edition, February 2018) obtained from the official website of Axis-Shield Density Gradient Media, a brand of Alere Technologies AS (https://www.axis-shield-density-gradient-media.com/organelleindexes.htm), and the link of the protocol is: https://www.axis-shield-density-gradient-media.com/S35.pdf. For nonreducing gels, cells were lysed in lysis buffer without DTT and cell lysates were prepared with 2ME-free SDS loading buffer. Protein concentrations were determined using a Bradford protein assay kit (Sangon, Shanghai, China). The proteins were run in ExpressPlus™ PAGE gels (M42015C, GenScript, China) and then transferred to polyvinylidene difluoride membranes (Amersham Bioscience). After blocking with 5% fat-free milk at room temperature for 1 h, blots were incubated with primary antibody overnight at 4 °C. The next day, the blots were washed with Tris buffered saline Tween 20 and then incubated with secondary antibody for 1 h at room temperature. Proteins were visualized using enhanced chemiluminescence substrate (Tanon, Shanghai, China). Antibodies used in this work included anti-Flag (F1804, Sigma-Aldrich), anti-tubulin (BS1699, Bioworld), anti-GAPDH (G8795, Sigma-Aldrich) anti-GSDMD (ab209845, abcam), anti-caspase-1 (SC-515, Santa Cruz), anti-TfR1 (ab84036, abcam), and anti-P2X7 (#13809, Cell Signaling Technology). Secondary antibodies including anti-rat IgG, anti-mouse IgG, and anti-rabbit IgG were all purchased from Sigma-Aldrich.

Immunostaining

Cells grown on coverslips were first fixed in PBS with 4% paraformaldehyde (PFA) for 15 min, and then permeabilized in 0.1% Triton X-100 in PBS for 15 min. After blocking with 5% BSA for 1 h, cells were stained with ASC antibody (ab175449, abcam) and then Alexa Fluor 488-conjugated secondary antibody. Nuclei were counterstained with DAPI (Cell Signaling). Images were captured at room temperature using a confocal microscope (FV-1000, Olympus).

FRET assay

HEK293T cells cultured on poly-lysine-coated (50 ng/mL) confocal dish were transfected with CFP- and YFP-GSDMD in a ratio of 3 to 1. To accumulate adequate fluorescence, 10 mM $MgSO_4$ was added immediately after the transfection. FRET signal was detected and analyzed by the FRET sensitized emission approach (Leica Microsystems Inc.) 16 h later, before and after a washout of Mg^{2+}.

Live-cell imaging

To examine cell death morphology, cells were treated as indicated in the six-well plates. Static brightfield images of pyroptotic cells were captured using an Olympus IX71 microscope.

For PI staining, 1 µg/mL PI dye obtained from an Annexin V-FITC/PI Apoptosis Detection Kit (catalog no. A211-01, Vazyme) was added right after the electroporation or nigericin stimulation. Images were captured using a confocal microscope (FV-1000, Olympus) 60 min later.

For Ca^{2+} signaling detection, cells were transfected with Ca^{2+} indicator GCaMP6 plasmid 24 h before imaging. The GCaMP6 fluorescence was excited using a 488 nm argon laser, and the images were recorded every 30 s using a confocal microscope (FV-1000, Olympus). Cells were incubated in a chamber with a 5% CO_2 atmosphere at 37 °C throughout the experiment. The average fluorescence intensity of the ROI was calculated using SV10-ASW software (Olympus). Image acquisition started immediately after doxycline addition (100 ng/mL).

ELISA

The amount of IL-1β in cell culture supernatants was measured by ELISA according to the manufacturer's protocol. For iBMDMs, a Mouse IL-1 beta/IL-1F2 Quantikine ELISA Kit (Cat#MLB00C, R&D Systems) was used. For THP-1 cells, a Human IL-1 beta/IL-1F2 Quantikine ELISA Kit (Cat#DLB50, R&D Systems) was used.

Animal studies

C57BL/6 mice were provided by the Model Animal Research Center (MARC) of Nanjing University (Nanjing, Jiangsu Province, China) and were housed in a specific pathogen-free

facility accredited by Association for Assessment and Accreditation of Laboratory Animal Care International.

6- to 8-week-old male mice were primed with 0.4 mg/kg *E. coli* O111:B4 LPS intraperitoneally (i.p.) and then challenged 6 h later with 10 mg/kg *E. coli* O111:B4 LPS i.p. Upon the secondary challenge, LPS was mingled with 1 mmol/kg $MgSO_4$, $MgCl_2$, $MgGluc_2$, or equal volume 0.9% NaCl as indicated. At indicated time points, mice were euthanized and whole blood was collected by cardiac puncture using the EDTA-2K tubes, and lung tissue was collected and fixed in 4% PFA solution. Subsequently, whole blood was used for hematological analysis, flow cytometry, and was centrifuged to provide plasma for the measurement of cytokines. Lung tissue was embedded in paraffin and sectioned, and H&E staining was performed according to the manufacturer's protocol (Cat#G1005, Servicebio).

Hematological analysis, flow cytometry, and measurement of plasma cytokines

Hematological analysis was performed using a Hemavet 950FS Hematology Analyzer (Drew Scientific, Miami Lakes, FL, USA) following the manufacturer's manual.

For flow cytometry, red blood cells (RBCs) were lysed using an RBC Lysis Buffer (Cat#00-4300, Invitrogen) and live cells/dead cells were discriminated using SYTOX Blue (Cat#S34857, Invitrogen). To assess cell types, CD11b-PE-CF594 (BD), Ly6G-BV421 (BD), Ly6C-FITC (BD), MHCII-APC-Cy7 (Biolegend), and F4/80-BV605 (Biolegend) antibodies were used for panel 1; CD3-FITC (BD), CD335-AF-647 (BD), CD4-APC-H7 (BD), CD8a-PE-CF594 (BD), and CD19-AF700 (Biolegend) antibodies were used for panel 2. Cells that stained were analyzed by flow cytometry (BD LSRFortessa™) and data were analyzed using FlowJo software.

For measurement of plasma cytokines (IL-1β, IL-6, TNF-α, IL-2, IL-4, IL-5, IL-10, IL-12p70, IFN-γ, KC/GRO), a V-PLEX Proinflammatory Panel 1 (mouse) Kit (Cat#K15048D-1, Meso Scale Diagnostics) was used and data were collected using a multiplex imager (QuickPlex SQ120, Meso Scale Diagnostics). However, the values of IL-6 and KC/GRO were excluded for exceeding the upper limits; thus, IL-6 was re-measured using a Mouse IL-6 Quantikine ELISA Kit (Cat#M6000B, R&D Systems) according to the manufacturer's protocol.

Statistics

Data are shown as mean ± SD using GraphPad Prism 7 Software (GraphPad Software, San Diego, CA). Unless otherwise specified, statistical analysis was performed using *t* test. The relationship between serum magnesium and monocyte percentage was assessed using a Pearson's correlation and then a linear regression analysis. Statistical analysis for survival was performed with log-rank (Mantel−Cox) test. $*P < 0.05$. $**P < 0.01$.

Study approval

Animal studies were approved by the MARC Animal Care and Use Committee. The clinical study was retrospective and did not involve interference with routine patient management. The institutional review board of Jinling Hospital indicated that ethical approval is not necessary and they indicated no objection for conducting this study.

Author contributions DW, JZ, and ZL conceived this study, designed the experiments and wrote the paper. DW performed most of the experiments, assisted by JZ, Qianyue C, PS, Qin C, YZ, DZ, QL, and JP. JZ, QH, and CZ collected and analyzed the clinical data, supervised by XW and JR ZL and XG supervised all research.

Compliance with ethical standards

References

1. Velissaris D, Karamouzos V, Pierrakos C, Aretha D, Karanikolas M. Hypomagnesemia in critically ill sepsis patients. J Clin Med Res. 2015;7:911–8.
2. Jiang P, Lv Q, Lai T, Xu F. Does hypomagnesemia impact on the outcome of patients admitted to the intensive care unit? A systematic review and meta-analysis. Shock. 2017;47:288–95.
3. Limaye CS, Londhey VA, Nadkart MY, Borges NE. Hypomagnesemia in critically ill medical patients. J Assoc Physicians India. 2011;59:19–22.
4. Soliman HM, Mercan D, Lobo SS, Melot C, Vincent JL. Development of ionized hypomagnesemia is associated with higher mortality rates. Crit Care Med. 2003;31:1082–7.
5. Thongprayoon C, Cheungpasitporn W, Erickson SB. Admission hypomagnesemia linked to septic shock in patients with systemic inflammatory response syndrome. Ren Fail. 2015;37:1518–21.
6. Weglicki WB. Hypomagnesemia and inflammation: clinical and basic aspects. Annu Rev Nutr. 2012;32:55–71.
7. de Baaij JH, Hoenderop JG, Bindels RJ. Magnesium in man: implications for health and disease. Physiol Rev. 2015;95:1–46.
8. Mazur A, Maier JA, Rock E, Gueux E, Nowacki W, Rayssiguier Y. Magnesium and the inflammatory response: potential physiopathological implications. Arch Biochem Biophys. 2007;458:48–56.

9. Schick V, Scheiber JA, Mooren FC, Turi S, Ceyhan GO, Schnekenburger J, et al. Effect of magnesium supplementation and depletion on the onset and course of acute experimental pancreatitis. Gut. 2014;63:1469–80.

10. Lee CY, Jan WC, Tsai PS, Huang CJ. Magnesium sulfate mitigates acute lung injury in endotoxemia rats. J Trauma. 2011;70:1177–85. discussion 85

11. Ahmed LA. Protective effects of magnesium supplementation on metabolic energy derangements in lipopolysaccharide-induced cardiotoxicity in mice. Eur J Pharm. 2012;694:75–81.

12. Eltanbouly DM, Abdelsalam RM, Attia AS, Abdelaziz MT. Pretreatment with magnesium ameliorates lipopolysaccharide-induced liver injury in mice. Pharmacol Rep Pr. 2015;67:914–20.

13. Kayagaki N, Warming S, Lamkanfi M, Vande Walle L, Louie S, Dong J, et al. Non-canonical inflammasome activation targets caspase-11. Nature. 2011;479:117–21.

14. Kovacs SB, Miao EA. Gasdermins: effectors of pyroptosis. Trends Cell Biol. 2017;27:673–84.

15. Kayagaki N, Stowe IB, Lee BL, O'Rourke K, Anderson K, Warming S, et al. Caspase-11 cleaves gasdermin D for non-canonical inflammasome signalling. Nature. 2015;526:666–71.

16. Hagar JA, Powell DA, Aachoui Y, Ernst RK, Miao EA. Cytoplasmic LPS activates caspase-11: implications in TLR4-independent endotoxic shock. Science. 2013;341:1250–3.

17. Kayagaki N, Wong MT, Stowe IB, Ramani SR, Gonzalez LC, Akashi-Takamura S, et al. Noncanonical inflammasome activation by intracellular LPS independent of TLR4. Science. 2013;341:1246–9.

18. Shi J, Zhao Y, Wang Y, Gao W, Ding J, Li P, et al. Inflammatory caspases are innate immune receptors for intracellular LPS. Nature. 2014;514:187–92.

19. Shi J, Zhao Y, Wang K, Shi X, Wang Y, Huang H, et al. Cleavage of GSDMD by inflammatory caspases determines pyroptotic cell death. Nature. 2015;526:660–5.

20. Mulvihill E, Sborgi L, Mari SA, Pfreundschuh M, Hiller S, Muller DJ. Mechanism of membrane pore formation by human gasdermin-D. EMBO J. 2018;37:e98321.

21. Ding J, Wang K, Liu W, She Y, Sun Q, Shi J, et al. Pore-forming activity and structural autoinhibition of the gasdermin family. Nature. 2016;535:111.

22. Liu X, Zhang Z, Ruan J, Pan Y, Magupalli VG, Wu H, et al. Inflammasome-activated gasdermin D causes pyroptosis by forming membrane pores. Nature. 2016;535:153–8.

23. Aglietti RA, Estevez A, Gupta A, Ramirez MG, Liu PS, Kayagaki N, et al. GsdmD p30 elicited by caspase-11 during pyroptosis forms pores in membranes. Proc Natl Acad Sci USA. 2016;113:7858–63.

24. Schmid-Burgk JL, Gaidt MM, Schmidt T, Ebert TS, Bartok E, Hornung V. Caspase-4 mediates non-canonical activation of the NLRP3 inflammasome in human myeloid cells. Eur J Immunol. 2015;45:2911–7.

25. Ruhl S, Broz P. Caspase-11 activates a canonical NLRP3 inflammasome by promoting K(+) efflux. Eur J Immunol. 2015;45:2927–36.

26. Wu Y, Ren J, Zhou B, Ding C, Chen J, Wang G, et al. Gene silencing of non-obese diabetic receptor family (NLRP3) protects against the sepsis-induced hyper-bile acidaemia in a rat model. Clin Exp Immunol. 2015;179:277–93.

27. Lee S, Nakahira K, Dalli J, Siempos II, Norris PC, Colas RA, et al. NLRP3 inflammasome deficiency protects against microbial sepsis via increased lipoxin B4 synthesis. Am J Respir Crit Care Med. 2017;196:713–26.

28. He WT, Wan H, Hu L, Chen P, Xin W, Zhe H, et al. Gasdermin D is an executor of pyroptosis and required for interleukin-1β secretion. Cell Res. 2015;25:1285–98.

29. Ross PE, Ehring GR, Cahalan MD. Dynamics of ATP-induced calcium signaling in single mouse thymocytes. J Cell Biol. 1997;138:987–98.

30. Virginio C, Church D, North RA, Surprenant A. Effects of divalent cations, protons and calmidazolium at the rat P2X7 receptor. Neuropharmacology. 1997;36:1285–94.

31. Mariathasan S, Weiss DS, Newton K, McBride J, O'Rourke K, Roose-Girma M, et al. Cryopyrin activates the inflammasome in response to toxins and ATP. Nature. 2006;440:228–32.

32. de Vasconcelos NM, Van Opdenbosch N, Van Gorp H, Parthoens E, Lamkanfi M. Single-cell analysis of pyroptosis dynamics reveals conserved GSDMD-mediated subcellular events that precede plasma membrane rupture. Cell Death Differ. 2018; 26:146–61.

33. Yang D, He Y, Munoz-Planillo R, Liu Q, Nunez G. Caspase-11 requires the Pannexin-1 channel and the purinergic P2X7 pore to mediate pyroptosis and endotoxic shock. Immunity. 2015;43:923–32.

34. Bruzzone S, Basile G, Chothi MP, Nobbio L, Usai C, Jacchetti E, et al. Diadenosine homodinucleotide products of ADP-ribosyl cyclases behave as modulators of the purinergic receptor P2X7. J Biol Chem. 2010;285:21165–74.

35. Hansen DB, Ye ZC, Calloe K, Braunstein TH, Hofgaard JP, Ransom BR, et al. Activation, permeability, and inhibition of astrocytic and neuronal large pore (hemi)channels. J Biol Chem. 2014;289:26058–73.

36. Cheng KT, Xiong S, Ye Z, Hong Z, Di A, Tsang KM, et al. Caspase-11-mediated endothelial pyroptosis underlies endotoxemia-induced lung injury. J Clin Invest. 2017;127:4124–35.

37. Russo HM, Rathkey J, Boydtressler A, Katsnelson MA, Abbott DW, Dubyak GR. Active caspase-1 induces plasma membrane pores that precede pyroptotic lysis and are blocked by lanthanides. J Immunol. 2016;197:1353.

38. Solle M, Labasi J, Perregaux DG, Stam E, Petrushova N, Koller BH, et al. Altered cytokine production in mice lacking P2X(7) receptors. J Biol Chem. 2001;276:125–32.

39. Morelli A, Chiozzi P, Chiesa A, Ferrari D, Sanz JM, Falzoni S, et al. Extracellular ATP causes ROCK I-dependent bleb formation in P2X7-transfected HEK293 cells. Mol Biol Cell. 2003;14:2655–64.

40. Ousingsawat J, Wanitchakool P, Schreiber R, Kunzelmann K. Contribution of TMEM16F to pyroptotic cell death. Cell Death Dis. 2018;9:300.

41. Platnich JM, Chung H, Lau A, Sandall CF, Bondzi-Simpson A, Chen HM, et al. Shiga toxin/lipopolysaccharide activates caspase-4 and gasdermin D to trigger mitochondrial reactive oxygen species upstream of the NLRP3 inflammasome. Cell Rep. 2018;25:1525–36 e7.

42. American College of Chest Physicians/Society of Critical Care Medicine Consensus Conference. Definitions for sepsis and organ failure and guidelines for the use of innovative therapies in sepsis. Crit Care Med. 1992;20:864–74.